Angular forces in group-VI transition metals: Application to W(100)

A. E. Carlsson
Department of Physics, Washington University, St. Louis, Missouri 63130
(Received 13 May 1991)

Quantum-mechanical analysis based on a tight-binding model is used to generate a functional form for angular forces in transition metals. Using a moment analysis, an expression is derived that includes angular forces via both explicit many-body interaction terms and a matrix description of a site's local environment. A fit based on this analysis, with only four fitting parameters, is used to treat Cr, Mo, and W. Calibration results for vacancy-formation energies and structural-energy differences are in excellent agreement with experiment and *ab initio* values. Application to the W(100) surface yields a physical picture of the $c(2\times2)$ reconstruction based on enhanced surface bond-strengthening effects. Agreement with *ab initio* results for the reconstruction amplitude and energy is obtained for reasonable values of the parameters, although both of these quantities depend on the cutoff radius.

INTRODUCTION

It has become clear over the past few years that an accurate description of interatomic forces in bcc transition metals necessitates the inclusion of angular terms. On the one hand, free-electron-based perturbative calculations[1-3] indicate that such terms are large in magnitude and make a major contribution to structural-energy differences. On the other hand, there have been several treatments[4,5] of the bcc transition metals using the "embedded-atom" format[6-8] and a matrix generalization thereof.[8a] Even though these are highly optimized, they generally obtain structural-energy differences which are much too small or even have the wrong sign.[5,8] This paper describes an approach to taking the next stop beyond the embedded-atom format in describing transition-metal energetics. This step is based on tight-binding analysis within a moment framework, which gives a natural sequence of locally based approximations for describing the energetics of transition metals. The intent is to establish the degree to which an extension including up to angular four-body interactions can describe bulk and defect energetics correctly. We treat only transition metals with nearly half-filled d bands. The method is simplest for these because approximate electron-hole symmetry allows one to ignore, to a first approximation, the effects of odd moments of the electronic density of states. The method we describe here is similar to one developed earlier[9] for Si. However, we find that it is possible to obtain accurate results without including electrostatic-dipole terms which were included in the Si method; these are expected to be less important in transition metals because of the short-ranged metallic screening that is present.

QUANTUM-MECHANICAL ANALYSIS AND PARAMETRIZATION

Our method is based on a tight-binding Hamiltonian of the form

$$H=\sum_{\substack{i,j\\ i\neq j}}\sum_{\alpha,\beta}h_{\alpha\beta}^{ij}|i,\alpha\rangle\langle j,\beta| \ , \tag{1}$$

where the $|i,\alpha\rangle$ are localized orthogonal atomiclike d orbitals on atomic sites i and the $h_{\alpha\beta}^{ij}$ are interatomic coupling strengths; α and β index the d orbitals on a particular site. The energy zero is chosen so that the on-site $i=j$ terms vanish. The effects of the s electrons are not included at this stage in order to keep the number of fitting parameters as small as possible. We believe that this is not a serious omission. A large number of tight-binding calculations have shown that, particularly for the half-filled d-band transition metals, the bulk of the structural energetics is contained in the d band.[10] Furthermore, at least part of the effects of the s electrons is included in the pair-potential repulsive term to be discussed later.

A local description of the electronic structure of this type of Hamiltonian is obtained via the moments

$$\mu_n(i)=\tfrac{1}{2}\int_{-\infty}^{\infty}E^n\rho_i(E)dE \ , \tag{2}$$

of the electronic density of states (DOS). Here i denotes a particular atomic site and $\rho_i(E)$ denotes the projected DOS on that site; the factor of one-half eliminates spin degeneracy. Thus $\mu_0(i)=5$. The μ_n are rigorously given[11] as sums of n-hop paths; for $n=4$, the highest-level moment to be included here, one has

$$\mu_4(i)=\sum_{j,k,l}\sum_{\alpha,\beta,\gamma,\delta}h_{ij}^{\alpha\beta}h_{jk}^{\beta\gamma}h_{kl}^{\gamma\delta}h_{li}^{\delta\alpha} \ . \tag{3}$$

At the level of the embedded-atom format, one includes only μ_2 in the energy function. This contains only radial pair terms and describes the mean-square width of the projected d DOS. For nearly-half-filled d-band transition metals, the next level at which significant new physics is obtained involves inclusion of μ_3 and μ_4. These describe the *shape,* as opposed to the *width,* of the DOS.[8,12] At a fixed value of μ_2,μ_3 describes the asymmetry of the DOS with respect to its center of gravity. μ_4 describes degree to which the DOS is divided into two distinct peaks, as opposed to a central peak. For small values of μ_4 (when appropriately scaled by μ_2), well-defined bonding and antibonding peaks can usually be revolved; such a DOS distribution may be thought of as

having a partly covalent character. On the other hand, large values of μ_4 correspond generally to a DOS dominated by a central peak. Electron-hole symmetry implies that μ_3 and the higher odd-order moments, do not contribute in first order to the energy[9] in the exactly half-filled band case. Furthermore, the numerical value of μ_3 in transition metals, when appropriately scaled by μ_2, is typically quite small.[13] Therefore, in the interest of simplicity, we ignore the μ_3 term and include only the effects of μ_4.

The first term in our energy function is similar to that used in Ref. 8a. It is based on $\hat{\mu}_2$ and has the form

$$E_{\rm el}^{(2)}=\sum_i E_{\rm el}^2(i)=-\sum_i \mathrm{Tr}[\hat{\mu}_2(i)^{1/2}] , \tag{4}$$

where

$$\mu_2^{\alpha\beta}(i)=\langle i,\alpha|H^2|i,\beta\rangle=\sum_{j,\gamma} h_{ij}^{\alpha\gamma}h_{ji}^{\gamma\beta} \tag{5}$$

is the second-moment *matrix*.[14] This part of the energy is relatively fast to compute, since by Eq. (5) $\hat{\mu}_2(i)$ is a collection of pair sums. Each term $E_{\rm el}^{(2)}(i)$ in $E_{\rm el}^{(2)}$ is simply minus the sum of the square roots of the eigenvalues of $\hat{\mu}_2(i)$. This form for the $\hat{\mu}_2$ energy can be derived from the matrix recursion method.[9,15] It reduces to the embedded-atom form in the single-orbital case and, also, for geometries in which all of the orbitals are equivalent. However, unlike the embedded-atom format, the $\hat{\mu}_2$ terms contain *angular* information about the local environment. $E_{\rm el}^{(2)}$ can, in fact, be described approximately by an angular three-body potential;[9,16] if only σ couplings are present, then the angular potential is proportional to $P_2(\cos\theta)^2$, where P_2 is a Legendre polynomial.[17] In cubic symmetry the eigenvalues split into a triply degenerate complex and a doubly degenerate one, giving the usual crystal-field splitting. In cases of higher symmetry (which occur only in icosahedral environments), $\hat{\mu}_2$ is a multiple of the identity matrix. In an arbitrary low-symmetry environment, the five eigenvalues are in general distinct.

There are also several model physical systems which are treated more accurately by $\hat{\mu}_2$ than by μ_2. For example, model studies[9,16] of Si indicate that the vacancy-formation energy in this system is obtained to much better accuracy by $\hat{\mu}_2$. In addition, the electronic-band-energy contribution to the binding energy of a transition-metal dimer molecule is obtained exactly by the $\hat{\mu}_2$ formulation, but not by the embedded-atom format. To show this, consider the basis $|i,m\rangle$ and $|j,m\rangle$ for the d orbitals on the atoms i and j in the molecule, where m is the usual azimuthal angular momentum quantum number and the axis of quantization is the bond axis. Then rotation about this axis is a symmetry of the Hamiltonian H, so that H couples $|i,m\rangle$ only to $|j,m\rangle$ and vice versa. Thus

$$\langle i,m|H^2|i,m'\rangle=\delta_{m,m'}h(m)^2 ,$$

where $h(m)=h_\sigma$ for $m=0$, h_π for $m=\pm1$, and h_δ for $m=\pm2$. Thus the eigenvalues of $\hat{\mu}_2(i)^{1/2}$ and $\hat{\mu}_2(j)^{1/2}$ are simply $|h(m)|$. Therefore, $E_{\rm el}^{(2)}(i)=E_{\rm el}^{(2)}(j)=-|h_\sigma|-2|h_\pi|-2|h_\delta|$, and the $E_{\rm el}^{(2)}$ estimate for the binding energy of the molecule is $=-2|h_\sigma|-4|h_\pi|-4|h_\delta|$. On the other hand, the two-atom Hamiltonian naturally breaks up into 2×2 blocks for each m; each of these blocks has two eigenvalues $\pm|h(m)|$. The binding energy of the molecule is obtained by placing two electrons in each of the lowest five levels, which yields a binding energy of $=-2|h_\sigma|-4|h_\pi|-4|h_\delta|$. Thus the $E_{\rm el}^{(2)}$ energy is exact for the dimer molecule. Although tests that we have performed indicate that the matrix character of $\hat{\mu}_2$ is not important for transition-metal point defects and surface structure, it may well be important for treating grossly undercoordinated configurations such as those which might occur in surface diffusion.

Although μ_4 contains up to four-body interactions, a part of it can be calculated by performing only two-body calculations.[9] We define

$$\mu_4^{(2)}(i)=\sum_{j,l}\sum_{\alpha,\beta,\gamma,\delta} h_{ij}^{\alpha\beta}h_{ji}^{\beta\gamma}h_{il}^{\gamma\delta}h_{li}^{\delta\alpha} , \tag{6}$$

so that only paths returning to site i after the second hop are included. By using Eq. (5) this can be written in the form

$$\mu_4^{(2)}(i)=\mathrm{Tr}[\hat{\mu}_2(i)^2] .$$

The energy from this part of $\mu_4(i)$ is already included in $E_{\rm el}^{(2)}(i)$. This is most readily seen by examination of the DOS distribution which is used to generate $E_{\rm el}^{(2)}$. As mentioned above, this DOS is obtained via the matrix recursion method; with a continued fraction truncated after the first level, this gives a DOS distribution of the form

$$\rho^{(2)}(E)=\sum_{\nu=1}^{5}[\delta(E-E_\nu)+\delta(E+E_\nu)] ,$$

where the E_ν are the square roots of the eigenvalues of $\hat{\mu}_2(i)$ (The results to be demonstrated are actually independent of the termination method; the truncation choice employed here is used because it yields the simplest algebra.) From Eq. (2) one readily shows that, for this DOS distribution, $\mu_4=\sum_{\nu=1}^5 E_\nu^4$. On the other hand, by the definition of the E_ν, the eigenvalues of $\hat{\mu}_2(i)$ are simply E_ν^2. Thus the eigenvalues of $\hat{\mu}_2(i)^2$ are E_ν^4; since the trace of a matrix is simply the sum of its eigenvalues, $\mu_4^{(2)}=\sum_{\nu=1}^5 E_\nu^4$. Comparing with the above results for $\rho^{(2)}$, we have that the value of μ_4 associated with $\rho^{(2)}$ is simply $\mu_4^{(2)}$. Therefore, the DOS generating $E_{\rm el}^{(2)}$ already has the value $\mu_4^{(2)}$ of μ_4, and corrections to the $E_{\rm el}^{(2)}$ term should contain only the *deviation* of μ_4 from $\mu_4^{(2)}$.

We find that $\mu_4^{(2)}$ typically contains only roughly half of μ_4, so that the corrections to $E_{\rm el}^{(2)}$ are clearly necessary. Thus we include another term which contains $\mu_4-\mu_4^{(2)}$:

$$E_{\rm el}^{(4)}=B\sum_i[\mu_4(i)-\mu_4^{(2)}(i)]/\mu_2(i)^{3/2} . \tag{7}$$

Here B is an adjustable constant. The factor of $\mu_2^{3/2}$ in the denominator is obtained via dimensional analysis; it is also given by treatments[18] based on model DOS distributions fitted to μ_2 and μ_4. In general, the electronic bind-

ing energy obtained by such model DOS distributions is a nonlinear function of μ_2 and μ_4; however, the nonlinearity in the μ_4 dependence of the energy in model DOS calculations is not very strong.[13] Therefore, in the interest of simplicity, we linearize this dependence as in Eq. (7). We find that inclusion of the $E_{\rm el}^{(4)}$ term leads to significantly improved structural-energy differences.

Finally, we include a phenomenological repulsive pair-potential term to counter the attractive electronic energy. Thus the total energy has the form

$$E=E_{\rm rep}+E_{\rm el}^{(2)}+E_{\rm el}^{(4)} , \tag{8}$$

where

$$E_{\rm rep}=\frac{1}{2}\sum_{i,j}V_2^{\rm rep}(i,j) .$$

To specify our model completely, it is necessary to give the interatomic coupling strengths and the radial form of $V_2^{\rm rep}$. The coupling strengths $h_{ij}^{\alpha\beta}$ are given via the usual Slater-Koster[19] relations in terms of interatomic couplings of σ, π, and δ symmetries. We assume the "canonical" ratios[20] of $6:-4:1$ for $h_\sigma:h_\pi:h_\delta$. The radial dependence of the d couplings in the $\hat{\mu}_2$ term is given as the following double integral:

$$h(r)=\begin{cases} A\int\int \exp[-(kr)^2]dr-a+b(r_1-r) , & r<r_1 \\ 0, & r\geq r_1 . \end{cases} \tag{9}$$

This form guarantees that both the first and second derivatives of h are monotonically decreasing with distance; this is important, because these determine the forces and force constants. The constants a and b are chosen to make both $h(r)$ and dh/dr go to zero smoothly at the cutoff radius r_1. The Gaussian integrand is chosen because this gives a more rapid large-r cutoff than many other possible forms, such as exponential and power-law decays. We use the double integral because otherwise monotonicity of the derivatives is not guaranteed. The same form of radial function is chosen for $V_2^{\rm rep}$.

Because the multiplicity of the $E_{\rm el}^{(4)}$ terms is high, we have used a simpler form for their radial dependence to reduce computation time:

$$h(r)=\begin{cases} h_0(r_2-r)^2 , & r<r_2 \\ 0, & r\geq r_2 . \end{cases} \tag{10}$$

In addition, the cutoff is chosen such that $r_2<r_1$. This form is used for both the μ_4 and μ_2 factors in Eq. (7). Thus the Hamiltonian matrix elements that are used in the $E_{\rm el}^{(4)}$ terms are somewhat different from those in the $E_{\rm el}^{(2)}$ terms. Although this causes some loss in accuracy, we feel that this loss is more than made up for by the gain in computation time, which is roughly two orders of magnitude.

Given this form, one would have five parameters to fit: two prefactors $A_{\rm el}^{\sigma}$ and $A_{\rm rep}$ for the electronic and repulsive terms, the two associated decay constants $k_{\rm el}$ and $k_{\rm rep}$, and the angular prefactor B [The constant h_0 in Eq. (10) is not an additional parameter, because varying it is equivalent to varying B in Eq. (7).] To reduce the number of free parameters, we make the further restriction that $k_{\rm rep}=2.5k_{\rm el}$. This provides for a reasonable balance between the attractive and repulsive terms. Comparison of calculated electronic-band energies and cohesive energies[21] suggests that the repulsive terms cancel less than 50% of the electronic-band energy in nearly-half-filled-band transition metals. We find that, if the restriction on the decay rates is not made, there is a tendency for cancellations of 70%–80% or more to occur. We consider such cancellations to be unphysical. The values of the four remaining parameters were obtained by a least-squares fit to a database comprised of the cohesive energy, equilibrium lattice constant, and three independent elastic constants for each metal. The values of the parameters are given in Table I. We note that the number of parameters here is smaller than is typically used in radial methods with the embedded-atom format, even though the energy function has considerably more richness.

RESULTS

The first set of calculations are aimed at assessing the overall accuracy of the method in calculating broken-bond energies and structural-energy differences. We take $r_1=6.0$ Å for W and Mo; for Cr the cutoff is scaled by the lattice constants. For r_2 we take a value of 4.2 Å for W, using scaled values for Cr and Mo; sensitivity tests for W are described below. The results for the vacancy-formation energies and bcc-fcc energy differences are given in Table II. The three cutoff distances used in the sensitivity tests for W are between the second-neighbor distance 3.16 Å and the third-neighbor distance 4.47 Å. It is convenient to think of these cutoffs as corresponding

TABLE I. Values of parameters in the angular force method. Note that B is dimensionless. Three different values of r_2 (which is not a fitting parameter) are used for W.

	Cr	Mo	W		
r_2 (Å)	3.829	4.187	4.0	4.2	4.4
$A_{\rm el}^{\sigma}$ (eV)	7.914	9.990	11.101	12.191	13.027
$A_{\rm rep}$ (eV)	773.1	368.6	341.3	371.3	373.6
$k_{\rm el}$ (Å^{-1})	0.4015	0.3242	0.3133	0.3148	0.3132
B	4.936	3.477	3.655	3.296	2.888

TABLE II. Calibration tests for vacancy-formation energy ε_v^f and structural-energy difference $\Delta E_{\text{bcc}-\text{fcc}}$ (per atom). Vacancy calculations include relaxation of nearest-neighbor shell. r_2 is the cutoff distance in the $E_{\text{el}}^{(4)}$ terms.

	Cr	Mo		W	
r_2 (Å)	3.829	4.187	4.0	4.2	4.4
ε_v^f (eV)					
Present	2.2	3.4	4.1	4.2	4.4
Expt.	2.0[a]	3.0[b]		4.0[b]	
$\Delta E_{\text{bcc}-\text{fcc}}$ (eV)					
Present	−0.38	−0.40	−0.45	−0.46	−0.47
Ab initio	−0.40[c]	−0.44[d]		−0.53[e]	

[a] Reference 22.
[b] Reference 23.
[c] Reference 24.
[d] Reference 25.
[e] Reference 26.

to different effective exponents in $1/r^n$ decay laws, where n is determined by forcing the algebraic decay law to obtain the same ratio of second- to first-neighbor couplings as is given by Eq. (10). It is readily seen that

$$n = 2\ \ln[(r_2 - r_{\text{NN}})/(r_2 - r_{\text{2NN}})]/\ln(r_{\text{2NN}}/r_{\text{NN}})\ ,$$

where r_{NN} and r_{2NN} are the first- and second-neighbor distances. Using the bcc ratio $r_{\text{NN}}/r_{\text{2NN}} = \sqrt{3}/2$, one finds that $n = 5.67$ for $r_2 = 4.0$ Å, $n = 4.75$ for $r_2 = 4.2$ Å, and $n = 4.08$ for $r_2 = 4.4$ Å.

All of the calculated vacancy-formation energies are within the error bars of the experimental measurements.[22,23] They are also fairly insensitive to the choice of cutoff radius. These results are in line with previous studies of broken-bond properties, which show that a large part of these energies comes from the reduction in local electron bandwidth;[7] this is described already by $\hat{\mu}_2$ (or even by the scalar μ_2). The structural-energy results are more surprising, however. These are within 15% of the *ab initio* estimates[24–26] and are also essentially independent of the cutoff radius. This is remarkable, in view of the fact that no structural-energy information was in the input database. The bcc-fcc energy difference is due almost entirely to the $E_{\text{el}}^{(4)}$ terms; in fact, the net contribution of the remaining terms favors the fcc structure. However, μ_4-based calculations using model DOS distributions typically obtain at most 60–70% of the *ab initio* values.[8,27] It is likely that the more accurate values obtained here are partly due to the use of empirical input quantities. The input quantity that seems to be the most closely associated with the angular forces is shear elastic constant $C' = (C_{11} - C_{12})/2$. The lattice distortion associated with this elastic constant does not change nearest-neighbor bond lengths to first order, and thus it is likely that angular effects make a large contribution to C'. We have, in fact, found that changing the input values of C' can cause large changes in the calculated structural-energy differences.

Our second set of calculations is aimed at obtaining a real-space description of the factors determining the structure of the W(100) surface. Surface relaxation properties are strongly affected by many-atom interactions in metals.[28–30] The breaking of the surface bonds leads to the strengthening[31] of "back bonds," which typically leads to a contraction of the first interlayer spacing. Effects of this type are naturally included in the embedded-atom format via the nonlinear dependence of the energy on the density of the local environment. Our results for the W(100) surface relaxation, in the absence of reconstruction, are shown in Fig. 1, using $r_2 = 4.2$ Å. In this analysis and in the subsequent analysis of reconstruction, we treat only first-layer displacements. The sum of the $E_{\text{el}}^{(2)}$ and E_{rep} terms favors the relaxation, as is

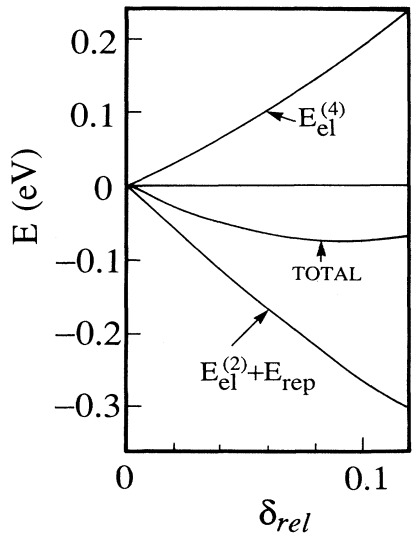

FIG. 1. Energetics of surface relaxation for the W(100) surface, including only first-layer motions. Displacement is in Å; energy is per surface atom.

expected from previous results with "embedded-atom" potentials.[30] In contrast, the four-body terms oppose the relaxation. The equilibrium contraction is 0.10 Å, with a relaxation energy of −0.08 eV/atom. Because the actual surface reconstructs, there are no experimental results to which to compare these numbers. For this reason we compare our results to *ab initio* results[32–36] instead (cf. Table III). We again use three different values of r_2 as a sensitivity test. Both the equilibrium contraction and relaxation energy are quite insensitive to the value of r_2. For all of the values of r_2, the first-layer contraction is very close to the *ab initio* results. The relaxation energy is also within the apparent "error bars" of the *ab initio* results. The surface energies are somewhat lower than the *ab initio* results and vary by roughly 15% with changing values of r_2.

The physics behind reconstructions, in contrast to relaxations, is not in general given by embedded-atom formulations. In fact, calculations with the embedded-atom format have not obtained the reconstructions observed on W and Mo surfaces.[30] The W(100) surface undergoes[37] a $c(2\times2)$ reconstruction. In the most widely believed model[38] for this reconstruction, alternate atoms are displaced in the (0,1,1) and (0, −1, −1) directions in the surface plane. This results in the formation of zigzag chains along the surface, with some bonds being lengthened and some being shortened. A large number of theoretical calculations have been performed for this system, ranging from fairly empirical approaches to completely *ab initio* calculations. We do not have space to review all of these here, but an extensive summary and list of references is given in Ref. 36. In general, two types of physical pictures have been emphasized. The first involves long-ranged interactions resulting from "nesting" of the Fermi surface,[39] which leads to greatly enhanced values of the electronic susceptibility at particular wave vectors. Such nesting has not been explicitly demonstrated, although some calculations[40] have indicated a strong wave-vector dependence of the surface phonon frequencies, with some of them becoming imaginary and providing an instability. The second picture involves surface bond-strengthening effects.[36,41] In this picture the strengthened surface bonds cause the second-neighbor atoms on the surface to move closer to each other, as occurs in the observed reconstruction. As mentioned above, such effects are naturally included in embedded-atom formulations. Since the observed W(100) reconstruction is not obtained by these formulations, it is apparently necessary to have more pronounced bond-strengthening effects than are obtained in the embedded-atom formulation. Surface bond strengthening has been observed in both charge densities obtained via *ab initio* calculations[36] and force constants obtained in tight-binding calculations.[41] At this point it has not been conclusively established which of the two mechanisms, long or short ranged, is the dominant one.

Our results for the $c(2\times2)$ reconstruction are shown in Fig. 2 for $r_2=4.2$ Å. In order to establish the physics as clearly as possible , only lateral displacements are included. The situation if precisely the reverse of the case for relaxations. The $E_{el}^{(2)}$ and E_{rep} terms in combination oppose the reconstruction, while the $E_{el}^{(4)}$ terms favor it.

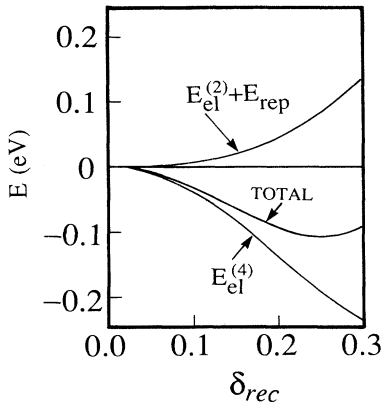

FIG. 2. Energetics of $c(2\times2)$ surface reconstruction for the W(100) surface. Reconstruction amplitude is δ_{rec}. Only lateral motions of first surface layer are allowed. Displacement is in Å; energy is per surface atom.

The optimal reconstruction amplitude δ is 0.25 Å, with an associated energy stabilization of −0.11 eV per surface atom. This number is given relative to the *unrelaxed* surface; the energy difference between the reconstructed and relaxed surfaces, which is sometimes referred to as the "reconstruction energy," is much smaller (−0.03 eV in this case). The physical picture behind the results obtained here corresponds most closely to the surface bond-strengthening mechanism discussed above. Changes in the $E_{el}^{(4)}$ terms come from changes in both μ_4 and μ_2. If μ_2 is fixed, then by Eq. (7), a decrease in μ_4 provides a stabilizing contribution. On the other hand, if μ_4 is fixed, then an increase in μ_2 provides a stabilizing contribution. Since μ_2 is determined completely by the number and distances of the near neighbors (and not their *angles),* the stabilizing contribution associated with increasing μ_2 corresponds to an enhanced surface bond strength, above and beyond what is already contained in the $E_{el}^{(2)}$ terms. This enhancement is the dominant effect here.

This is illustrated in Fig. 3, which shows $E_{el}^{(4)}$, $\mu_4^c=\mu_4-\mu_4^{(2)}$, and $\gamma_4^c=\mu_0\mu_4^c/(\mu_2)^2$ in the first two surface layers, as well as the bulk values. For the first two layers, the left-hand (dashed) bar indicates the value for the ideal surface, while the right-hand (solid) bar indicates the value for the reconstructed surface. The quantity γ_4^c provides a measure of the shape of the DOS; according to the μ_4 discussion above, small values of γ_4^c corresponds to a two-peaked structure for the DOS and large values correspond to a single peak at the center of the band. The factor of μ_0 ensures that γ_4^c is independent of the overall normalization of the DOS. The value of $E_{el}^{(4)}$ is strongly enhanced at the surface. This enhancement can be associated with the increased surface value of γ_4^c, seen in the middle frame, since $E_{el}^{(4)}=B\gamma_4^c\mu_2^{1/2}$. The large surface value of γ_4^c corresponds to a value of the DOS at the Fermi level which is higher than what would already be expected from the surface reduction in μ_2. Upon reconstruction, $E_{el}^{(4)}$ in the surface layer is reduced; this reduction, in fact, accounts for most of the energy stabilizing

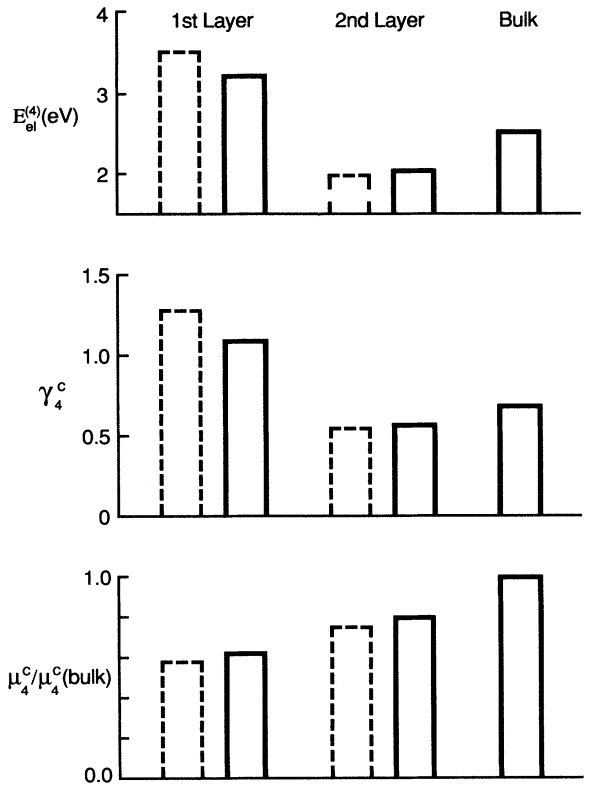

FIG. 3. Four-body energy $E_{el}^{(4)}$, band-shape parameter γ_4^c, and part μ_4^c of fourth moment for W(100) surface layers for $r_2=4.2$ Å. Dashed bars indicate values in absence of reconstruction or relaxation; solid bars indicate values for reconstruction of amplitude 0.25 Å, with only lateral displacements.

the reconstruction (cf. Fig. 2). The drop in $E_{el}^{(4)}$ is associated with a reduction in γ_4^c. This reduction, in turn, is due to a reconstruction-induced *increase* in μ_2 rather than a *decrease* in μ_4^c; in fact, as is seen in Fig. 2, μ_4^c increases upon reconstruction. Thus our results support the enhanced bond-strengthening mechanism discussed above. Surface states may play an important role here. The increased value of γ_4^c at the surface is likely due in part to surface states,[18] which have been found in the *ab initio* calculations.[33,36] Thus the drop in γ_4^c upon reconstruction may correspond to the elimination of some of the surface-state peak. We note that the angular character of the contributions to μ_4^c is still important. If, for example, the various paths contributing to μ_4^c all contributed with the same sign (as would be the case in an *s*-band model), then μ_4^c would be expected to be roughly proportional to $(\mu_2)^2$. $E_{el}^{(4)}$ would then *increase,* rather than decease, as a result of the reconstruction. The constancy of μ_4^c is partly due to the cancellation effects resulting from different paths having opposite signs.

Table III provides comparison with *ab initio* results and sensitivity analysis for the reconstruction. Here both lateral and perpendicular displacements are included in our results. Unfortunately, there is no unique set of *ab initio* results, since there are large discrepancies between *ab initio* results (the two full-potential linear augmented-plane-wave lines in the table) obtained via similar methods by different groups. For $r_2=4.2$ and 4.4 Å, the calculated reconstruction amplitude and magnitude are consistent with the *ab initio* results (within the large apparent error bars of the latter); they are also consistent with the rather uncertain experimental data,[42] which place the reconstruction amplitude between 0.15 and 0.30 Å. However, in the case of $r_2=4.0$ Å, the calculated reconstruction amplitude is much too small. Thus obtaining the correct structure is not guaranteed by the

TABLE III. Calculated properties of the W(100) surface. Energies E_{rel} and E_{rec} resulting from relaxation and reconstruction are in eV per surface atom and are measured relative to the ideal unrelaxed surface. Displacements δ are in Å; negative values of δ_{rel} denote inward displacements. $E_{rec}^{(0)}$ and $\delta_{rec}^{(0)}$ obtained including only lateral displacements; E_{rec} and δ_{rec} include both perpendicular and lateral displacements of first layer. E_{surf} denotes surface energy in eV per surface atom. The first three lines give present estimates. "PP" denotes *ab initio* pseudopotential calculations; "FLAPW" denotes *ab initio* full-potential linear-augmented-plane wave calculations. Present estimates of E_{surf} include both perpendicular and lateral displacements; PP estimate includes only relaxation effects (perpendicular displacements).

	E_{rel}	δ_{rel}	$E_{rec}^{(0)}$	$\delta_{rec}^{(0)}$	E_{rec}	δ_{rec}	E_{surf}
$r_2=4.0$	−0.07	−0.10	−0.05	0.19	−0.07	0.05	2.5
$r_2=4.2$	−0.08	−0.10	−0.11	0.25	−0.11	0.22	2.7
$r_2=4.4$	−0.07	−0.09	−0.16	0.28	−0.16	0.28	2.9
PP[a]	−0.06	−0.09					3.1
FLAPW[b]	−0.05	−0.09			−0.09	0.19	
FLAPW[c]	−0.05	−0.09	−0.15	0.27	−0.15		3.3

[a] Reference 32.
[b] References 33 and 34.
[c] References 35 and 36.

present method, although it is obtained for reasonable values of the parameters. We believe that a major part of the effect of changing r_2 comes from changing in the ratio of the second- to first-neighbor couplings. For $r_2=4.0$, 4.2, and 4.4 Å, Eq. (10) implies that this ratio has the values 0.442, 0.505, and 0.556, respectively. Since the $\mu_2^{3/2}$ term in Eq. (7) contains these couplings to the third power, differences in second-neighbor coupling strengths can cause substantial differences in $E_{\rm el}^{(4)}$. It is generally believed that d-orbital couplings follow roughly a $1/r^5$ decay law.[20] This gives a second- to first-neighbor coupling ratio of 0.487, which would be obtained for $r_2=4.14$ Å. Interpolation of the reconstruction energies given in Table III suggests that this value would provide an accurate treatment of the reconstruction. However, the $1/r^5$ decay is not exact. We feel that the most reliable procedure for treating surfaces within the present method is to choose a value of r_2 that gives a reconstruction energy consistent with the *ab initio* results.

CONCLUSIONS

In summary, the method described here gives a good description of both bulk and surface structural energetics, despite the small number of fitting parameters that are used. Both the broken-bond physics determining vacancy-formation energies and surface relaxations and the DOS-shape physics that determines structural-energy differences are obtained in a fashion that is fairly insensitive to the precise form of fit that is used. The tendency of the W(100) surface to reconstruct is also fairly fit independent; however, the reconstruction amplitude and energy are sensitive to the choice of fit. We believe that the present angular force method is sufficiently accurate to provide insight into a variety of materials properties. Simulations of such properties, if done via molecular dynamics, require the forces or gradients of the total-energy function. We have obtained these by analytic differentiation of the various radial and angular functions that enter the total energy, which increases the computation time by roughly a factor of 5. At this point it is not clear which properties will be most sensitive to the types of angular terms included here. It is widely believe that the structures of closely packed defects, such as dislocations, are primarily determined by hard-core packing effects. This belief can now be tested by explicit calculations with angular forces. Our results for the W(100) surface would suggest that the effects of angular forces on structure are largest when broken bonds are present. The total-energy method we have described is sufficiently fast that it should be possible to perform realistic finite-temperature simulations of surface structure and other materials properties involving such broken bonds.

ACKNOWLEDGMENTS

I am grateful to Murray Daw, Steven Foiles, Tom Felter, and Rob Phillips for enlightening conversations. Richard Watson generously supplied unpublished structural-energy results. This work was supported by the Department of Energy under Grant No. DE-FG02-84ER45130.

[1]J. A. Moriarty, Phys. Rev. Lett. **55**, 1502 (1985).
[2]J. A. Moriarty, Phys. Rev. B **38**, 3199 (1988).
[3]J. A. Moriarty and R. B. Phillips, Bull. Am. Phys. Soc. **35**, 283 (1990).
[4]M. W. Finnis and J. M. Sinclair, Philos. Mag. A **50**, 45 (1984); **53**, 161 (1986).
[5]J. B. Adams and S. M. Foiles, Phys. Rev. B **41**, 3316 (1990), and references cited therein.
[6]M. S. Daw and M. I. Baskes, Phys. Rev. Lett. **50**, 12 385 (1983); Phys. Rev. B **29**, 6443 (1984).
[7]See V. Heine, in *Advances in Research and Applications,* Vol. 35 of Solid State Physics, edited by H. Ehrenreich and D. Turnbull (Academic, New York, 1980) p. 1.
[8]See also A. E. Carlsson, in *Advances in Research and Applications,* Vol. 43 of Solid State Physics, edited by H. Ehrenreich and D. Turnbull (Academic, New York, 1990), p. 1.
[8a]J. D. Kress and A. F. Voter, Phys. Rev. B **43**, 12 607 (1991).
[9]A. E. Carlsson, P. A. Fedders, and C. W. Myles, Phys. Rev. B **41**, 1247 (1990).
[10]See D. G. Pettifor, in *Physical Metallurgy,* edited by R. W. Cahn and P. Haasen (North-Holland, New York, 1983) p. 73.
[11]F. Cyrot-Lackmann, J. Phys. Chem. Solids **29**, 1235 (1968).
[12]See J. P. Gaspard and P. Lambin, in *The Recursion Method and Its Applications,* edited by D. G. Pettifor and D. L. Weaire (Springer, New York, 1985), p. 72.
[13]R. H. Brown and A. E. Carlsson, Phys. Rev. B **32**, 6125 (1985).
[14]J. Inoue and Y. Ohta, J. Phys. C **20**, 1947 (1987).
[15]R. Jones and M. Lewis, Philos. Mag. B **49**, 95 (1984).
[16]A. E. Carlsson, in *Many-Atom Interactions in Solids,* edited by R. M. Nieminen, M. J. Puska, and M. J. Manninen (Springer, New York, 1990), p. 257.
[17]This follows from the analysis of K. Hirai and J. Kanamori, J. Phys. Soc. Jpn. **50**, 2265 (1981).
[18]R. H. Brown and A. E. Carlsson, Solid State Commun. **61**, 743 (1987).
[19]These are conveniently summarized in W. A. Harrison, *Electronic Structure and the Properties of Solids* (Freeman, New York, 1980).
[20]H. L. Skriver, *The LMTO Method* (Springer, New York, 1984).
[21]V. L. Moruzzi, J. F. Janak, and A. R. Williams, *Calculated Electronic Properties of Metals* (Pergamon, New York, 1987).
[22]G. D. Loper, L. C. Smedskjaer, M. K. Chason, and R. W. Siegel, in *Positron Annihilation,* edited by P. C. Jain, R. M. Singru, and K. P. Gopinathan (World Scientific, Singapore, 1985), p. 461.
[23]K. Maier, M. Peo, B. Saile, H. E. Schaefer, and A. Seeger, Philos. Mag. A **40**, 701 (1979).
[24]H. L. Skriver, Phys. Rev. B **31**, 1909 (1985).
[25]R. E. Watson (private communication).
[26]G. W. Fernando, R. E. Watson, M. Weinert, Y. J. Wang, and J. W. Davenport, Phys. Rev. B **41**, 11 813 (1990).
[27]P. Turchi, and F. Ducastelle, in *The Recursion Method and Its*

Applications, edited by D. G. Pettifor and D. L. Weaire (Springer, New York, 1985), p. 104.
[28]S. M. Foiles, M. I. Baskes, and M. S. Daw, Phys. Rev. B **33**, 7893; **37**, 10 378 (1988).
[29]G. J. Ackland, G. Tichy, V. Vitek, and M. W. Finnis, Philos. Mag. A **56**, 735 (1987).
[30]G. J. Ackland and M. W. Finnis, Philos. Mag. A **54**, 301 (1986).
[31]D. Tomanek and K. H. Bennemann, Surf. Sci. **163**, 503 (1985).
[32]C. T. Chan and S. G. Louie, Phys. Rev. B **33**, 2861 (1986).
[33]C. L. Fu, A. J. Freeman, and E. Wimmer, Phys. Rev. Lett. **54**, 2261 (1985).
[34]C. L. Fu and A. J. Freeman, Phys. Rev. B **37**, 2685 (1988).
[35]D. Singh, S.-H. Wei, and H. Krakauer, Phys. Rev. Lett. **57**, 3292 (1986).
[36]D. Singh and H. Krakauer, Phys. Rev. B **37**, 3999 (1988).
[37]T. Felter, R. A. Barker, and P. J. Estrup, Phys. Rev. Lett. **38**, 1138 (1977).
[38]M. K. Debe and D. A. King, Phys. Rev. Lett. **39**, 708 (1977); Surf. Sci. **81**, 193 (1979).
[39]E. Tosatti, Solid State Commun. **25**, 637 (1978).
[40]X. W. Wang and W. Weber, Phys. Rev. Lett. **58**, 1452 (1987).
[41]D. P. Joubert, J. Phys. C **20**, 1899 (1987).
[42]R. A. Barker, P. J. Estrup, F. Jona, and P. M. Marcus, Solid State Commun. **25**, 375 (1978).